Rev. Mexicana Astron. Astrof., **22**, 27-41 (1991)

DISTRIBUTION AND STUDIES OF THE INFRARED STELLAR POPULATION IN THE GALAXY. I. THE MODEL

R. A. Ruelas-Mayorga

Instituto de Astronomía
Universidad Autónoma de México

Received 1990 August 3

RESUMEN

Hemos desarrollado un modelo para la distribución de las estrellas en nuestra galaxia, siguiendo los mismos lineamientos utilizados por Bahcall y Soneira (1980). Este modelo consiste de tres componentes estelares, y una componente la cual representa la capa absorbente (polvo) en el plano galáctico.

Las características de las componentes de este modelo son las siguientes:

i) La densidad estelar en el plano decae de una manera exponencial con la distancia radial al centro (R) y con la distancia perpendicular al plano (Z). La capa absorbente comparte también esta dependencia con R y Z.

ii) Observaciones infrarojas del bulbo galáctico muestran que su densidad puede ser representada de una manera apropiada por medio de una familia de esferoides oblatos con una razón de su eje menor al mayor de b/a $\sim$ 0.75.

iii) Un anillo denso, localizado a una distancia R = R_0 sin 25 del centro también es utilizado. Los efectos de esta componente se observan solamente en direcciones en la vecindad de $l \sim 25$ y $l \sim 340$. Se supone también que este anillo es solamente un engrosamiento del disco, asi que donde el anillo está presente, la contribución del disco se toma como constante e igual en valor a aquella que existía en el punto externo del anillo con respecto al centro galáctico.

El modelo se usa para predecir las observaciones de flujo integrado a una longitud de onda de 2.4 μm en el intervalo $-70 \leq l \leq 60$ de modo que los valores de algunas constantes de la descripción matemática del modelo puedan ser determinados.

Subsecuentemente se usa el modelo con mucho éxito para predecir algunas cuentas estelares infrarojas en varias direcciones galácticas las cuales han sido obtenidas de la literatura.

ABSTRACT

Following the approach taken by Bahcall and Soneira (1980) we develop a model for the distribution of stars in our galaxy.

This model consists of three stellar components, and of one component which is intended to represent the absorption layer (dust) in the galactic plane.

The characteristics of this model's components are as follows:

i) The stellar density in the plane decays exponentially with radial distance from the centre (R) and with distance perpendicular to the plane (Z). The absorption layer shares also this dependence on R and Z.

ii) Infrared observations of the bulge show that its density may be well represented by a family of oblate spheroids with a ratio of minor to major axis equal to b/a $\sim$ 0.75.

iii) A dense ring, located at a distance R = R_0 sin 25 from the centre is also utilised. The effects of this component are noticeable only at galactic longitudes in the vicinity of $l \sim 25$ and $l \sim 340$. We also suppose that this ring is only an enhancement of the disk, so where the ring is present, the disk's contribution is taken as constant and equal to its value at the external point of the ring with respect to the galactic centre.

The model is used to predict the 2.4 μm flux observations in the interval $-70 \leq l \leq 60$ so that the values for several constants of its mathematical description could be fixed.

Subsequently the model is successfully used in predicting infrared stellar counts taken from the literature for different directions in the galaxy.

Key words: **GALAXY-STELLAR CONTENT – GALAXY-STRUCTURE – INTERSTELLAR-DUST**

I. INTRODUCTION

The observed distribution of the visible light in spiral galaxies has been accurately described in a number of papers, such as: de Vaucouleurs (1959), Freeman (1970), Kormendy (1977a,b), and van der Kruit and Searle (1981a,b; 1982a,b. These papers describe the spiral galaxies visual light distribution as made of two components; a thin disk which shows an exponential radial decay and which must be sharply cut off at a radius equal to a few times the radial scale length. The disk appears to extend all the way to the galactic centres. The second component is spheroidal in shape and, as is well known, it may appear with different degrees of importance, from very big and luminous bulges which dominate the bulk of the visual emission, to small and rather faint bulges which are difficult to differentiate from the disk component.

The projected light distribution of elliptical galaxies and that of spheroidal bulges of spiral galaxies has been described by de Vaucouleurs (1959), and Kormendy (1977a). It appears well represented by the $r^{1/4}$ law which takes the following mathematical form:

$$\log\left(I(\theta)/I(\theta_e)\right) = -3.3307\left((\theta/\theta_e)^{1/4} - 1\right) ,$$

where $I(\theta)$ represents the surface brightness observed at an angular distance equal to θ, and θ_e represents the effective radius which is defined as the distance within which half of the total radiation is emitted.

In the infrared (IR) wavelengths astronomers have gathered balloon observations at 2.4 μm. At this wavelength, the IR airglow shows a window (lack of emission), hence making it ideal for high signal to noise data gathering. Observations and discussion of these results may be found in the following papers: Hayakawa *et al.* (1976); Ito, Matsumoto and Uyama (1977); Hayakawa *et al.* (1977); Hofmann, Lemke and Thum (1977); Maihara, Oda and Okuda (1979), Hayakawa *et al.* (1979a, b); Okuda (1980); Hayakawa *et al.* (1981), and Matsumoto *et al.* (1982). Far IR studies of the galactic plane, and preliminary individual star-distribution IR studies of the galaxy may be found in the following papers: Maihara *et al.* (1979) (150 μm); Nishimura, Low and Kurtz (1980) (100-300 μm); Boissé *et al.* (1981) (71-95 μm) and (114-196 μm); Maihara *et al.* (1981) (150, 210 μm); Elias (1978a, b), Okuda (1980), Mikami and Ishida (1981), Ishida and Mikami (1982), Mikami *et al.* (1982), Kawara *et al.* (1982), and Hiromoto *et al.* (1983).

The main results of these studies show that both the near (2.4 μm) and far IR radiations have distributions along the galactic plane similar to those of other objects such as: the thermal continuum at 1.4 GHz and 5 GHz, the nonthermal continuum at 150 MHz, OH/IR stars, the 166α and 109α radio lines and γ-rays.

The near IR longitude profiles are similar in shape to the microwave CO profiles ($\lambda \sim 2.6$ mm), but the humps in the CO diagrams appear shifted with respect to those at the IR diagrams. Comparisons with the H I distribution show that the near IR radiation seems to be more predominant in the inner sections of the galaxy than that of the H I. Some of the humps and steps observed at 2.4 μm have been successfully associated with various spiral arms and close-by H II complexes. One of the remarkable features observed at 2.4 μm is the presence of two almost symmetrically located humps with respect to the galactic centre at longitudes of $l \sim 30$ and $l \sim 340$. These features have been associated with the 5 kpc (R_0 = 10 kpc) molecular ring apparent at radio wavelengths (Burton 1976).

The 2.4 μm radiation maxima do not lie exactly at b = 0, but appear consistently shifted to negative latitudes for the southern hemisphere. This "wiggling" of the galactic plane has also been observed for H I gas, H II regions, supernova remnants and molecular clouds (Lockman 1977, 1979) in the galactocentric distance range 6.5 kpc (R_0 = 10 kpc). This effect has also been noted for A-type stars along the galactic plane by Lyngå and Ruelas-Mayorga (1979).

The latitude distribution of IR radiation as well as that for the optical radiation shows that the disk component may be described as an exponential function of the height above the fiducial (b = 0) galactic plane $\exp(-Z/Z_0)$. For points closer to the galactic plane, theoretical calculations show that the perpendicular density distribution should be proportional to $\mathrm{sech}^2(Z/2Z_0)$. The optical studies by van der Kruit and Searle (1981a,b; 1982a,b) make use of this expression. It may be easily proved that for relatively high values of Z, $\mathrm{sech}^2(Z/2Z_0)$ tends to $\exp(-Z/Z_0)$, and since the IR-flux studies to date have been made with a large beam ($\sim 1.7°$) the difference between these mathematical expressions is insignificant. The galactic disk excluding the bulge appears to have a constant thickness along the whole range of galactic longitude observed; the perpendicular scale height Z_0 for optical studies of external galaxies turns out to be constant, this observation implies that the perpendicular velocity dispersion should decrease with radius along the disk. Corroboration that this is the case has been recently obtained by van der Kruit and Freeman (1984).

The 2.4 μm observations of the central regions of the galaxy show that the galactic bulge may be

described as an oblate spheroid, with its major axis (a) parallel to the galactic plane and with a ratio of minor axis (b) to major axis (a) equal to b/a ~ 0.75 (Matsumoto *et al.* 1982).

In what follows we shall develop a model for the stellar distribution in our galaxy based upon the current knowledge of our galaxy and of external spiral galaxies summarised in this section. Subsequently, this model is used to predict the 2.4 μm flux for the galaxy and then its predictions for stellar counts are compared with observations of selected areas along the galactic plane.

II. THE MODEL

The IR galaxy is described as a three component entity. The components are as follows: (1) a thin stellar disk, (2) a dense ring of radius equal to R_0 sin 25 and (3) an oblate spheroidal bulge. We have decided not to include in our model a thick disk similar to that discovered by Gilmore and Reid (1983) because this feature does not represent numerically a significant percentage of the total stellar population. Gilmore and Reid (1983) estimate that at the solar neighbourhood, the thick disk accounts for only 2% of the total number of stars.

a) *The Disk*

The disk component is represented by a thin disk of stars whose density decreases exponentially from the centre outward and perpendicularly from the galactic plane. The disk's stellar density at any point in the galaxy may be calculated as follows:

$$\rho(R,Z) = \rho_0 \exp\,[(R_0-R)/h]\,\exp(-Z/Z_0)\ ,$$

where this expression is valid for individual stellar spectral types. The term R_0 represents the distance from the galactic centre to the Sun which we have set at R_0 = 8.75 kpc as a result of an average of recent determinations of R_0 (see Graham 1979), ρ_0 represents the density of stars of a specific spectral type at the solar neighbourhood, Z_0 represents the scale height above the galactic plane for a specific spectral type. The Luminosity Function (LF) which we have used is that shown in Table A1. For column explanation see the Appendix. Most of the values were taken directly from Elias (1978a) except for the addition of late-type dwarfs (Faber *et al.* 1976; Allen 1973) and the stars in young OB associations. Values for young luminous stars were calculated from the tabulated data on luminous stars in the Milky Way by Humphreys (1978). The parameter h represents the radial scale length for the galactic disk, the value of this quantity has been determined from fitting the model flux predictions to the 2.4 μm radiation longitude profiles (see section III) and to particular cases of stellar counts determinations (see Ruelas-Mayorga and Teague 1991). The variables R and Z represent the distance from the galactic centre and the distance measured perpendicularly from the plane.

Changes in the parameters ρ_0, R_0, h and Z_0 cause equivalent variations in the predicted fluxes and values for the predicted Cumulative Counts Function (CCF) (log No. of stars per sq. deg. up to a specific magnitude vs. magnitude). A change of h from 3.1 to 2.5 kpc at the galactic centre produces a flux increase of $\sim 3 \times 10^{-10}$ W cm^{-2} μm^{-1} sr^{-1} which corresponds to a 57% increase. This increment of the flux shows as ~ 0.20 shift in the CCF. This type of shift is easily masked by the observational errors attached to stellar counts. At the same value of h, a change of R_0 from 8 kpc to 10 kpc changes the flux by a maximum factor of ~ 1.4. We conclude that reasonable uncertainties on these parameters produce variations of the total flux which are within a factor ≤ 2.

To preserve the relative proportions of the perpendicular and radial extents of the galactic disk (~ 1/10000), changes in Z_0 must be relatively small. Possible errors in the determinations of Z_0 for different spectral types will not have an important effect on the model predictions.

b) *The Absolute Magnitude Distribution*

Following Blaauw (1963) and Elias (1978a,b), we assume that the absolute magnitude of the stars at a specific spectral type is distributed around a mean value in a Gaussian form, therefore the relative number density function of stars which have absolute magnitude equal to M may be obtained as follows:

$$f(M) = (\sigma^{-1}\, 2^{-1/2}\, \pi^{-1/2} \exp(-(M-M_0)^2/2\sigma^2)\ ,$$

where M_0 and s represent the mean absolute magnitude and the dispersion around the mean for a group of stars of a specific spectral type. The absolute magnitudes and dispersions for the different spectral types for the 2.4 μm wavelength case are also shown in Table A1. A table containing the quantities R_0, Z_0, M_0 and σ for other wavelengths (*B*, *V*, *J*, *H*, *K*, 2.4 μm, *B–V*, *V–K*, *J–H*, *H–K*, and *J –K*) is given in the Appendix. Potentially this information may be used in conjunction with the model to predict fluxes and stellar count distributions at these alternative wavelengths. However, for the visual and blue bands, observational information of the same type used for the derivation of the model constants for the 2.4 μm case (see section III) would be necessary, since it is expected that radically different spectral types are responsible for the radiation at different spectral wavelengths. An indication of this fact may be found in the studies by Freeman (1970) and

van der Kruit and Searle (1981a,b; 1982a,b) which indicate that the radial scale length for the *B* and *V* cases are of the order 4 to 5 kpc, that is ~ 1.5 to 2 times larger than the radial scale length derived for the 2.4 μm case.

c) *Absorption Considerations*

Several models for the interstellar absorption within the galaxy have been proposed. For a quick description of these models see the paper by Bahcall and Soneira (1980) and the references therein. Other types of absorption models have been proposed by Hayakawa *et al.* (1977, 1981), based on the assumption that the absorption is proportional to the total column density of hydrogen (H I, H II, and H_2) particles along the line of sight. These models depend on the observed H I and CO densities, which in turn may be derived from the radio observations provided optical thinness is assumed and the ratios between $C^{12}O/C^{13}O$ are accurately known.

It seems to us that the number of assumptions required for the Hayakawa *et al.* model is too large and that its agreement with the observations may be purely fortuitous. This, of course, does not mean that these models are not appropriate for the purpose which they serve in the Hayakawa *et al.* papers.

The Bahcall and Soneira model contains a series of simple assumptions such as homogeneous distribution of absorbing matter, discontinuities in the density of absorbing matter toward the galactic poles, etc. They represent a first approximation to the distribution of the absorbing matter in the galaxy.

We think that an absorption model which allows for radial as well as perpendicular variations for the amount of absorption is more appropriate to the philosophy of the research presented in this paper.

Following Jones *et al.* (1981) we assume that the absorbing matter in the galaxy is distributed similarly to the stars in the disk, that is, it shows an exponential decay from the galactic centre as well as from the galactic plane.

It is also assumed that the absorbing matter is not present in the bulge component. The similarity between spiral galaxy bulges and elliptical galaxies, which in general lack dust, supports this assumption.

The absorption at any point in the galaxy may be calculated by using the following expression:

$$dA(R,Z) = a_0 \exp[(R_0-R)/h_{abs})] \exp(-Z/Z_{abs})dr ,$$

where this equation is valid for a single wavelength. a_0 represents the value of the absorption at the specific wavelength in the solar neighbourhood in units of mag kpc^{-1}. R, Z, h_{abs} and Z_{abs} are respectively the distance from the galactic centre, the distance from the galactic plane, the radial scale length for the absorbing matter along the galactic plane and the perpendicular scale length for the absorbing matter. Values of the determinations of a_0 for infrared as well as optical wavelengths have been quoted in numerous papers such as Hayakawa *et al.* (1977) and Johnson (1968).

The values of the constants h_{abs} and Z_{abs} have been adjusted so as to make the absorption model produce the values measured for the total absorption towards the galactic centre (Becklin and Neugebauer 1968) and towards the galactic poles (Bahcall and Soneira 1980). The values determined are as follows:

$$h_{abs} = 4.0 \text{ kpc}$$

$$Z_{abs} = 0.1 \text{ kpc} .$$

The relationship derived for the absorption at different IR wavelengths $a(\lambda) \sim \lambda^{-2.5}$ (Jones and Hyland 1980) and the ratios from the van de Hulst curve No. 15 (see Johnson 1968) allow the calculation of the $a_0(\lambda)$ for different wavelengths. In the Appendix the values of a_0 for the eleven wavelengths mentioned above are given.

The total 2.4 μm flux at a given position changes by a maximum factor of the order ~ 2.5 when the local absorption coefficient is changed from 0.08 mag kpc^{-1} to 0.04 mag kpc^{-1}. For a change in the absorption radial scale length from 4 kpc to 6 kpc the flux increases by a maximum factor of the order ~ 1.7. If the perpendicular scale length for the absorbing matter is changed from 0.05 kpc to 0.3 kpc, a maximum change in the flux of the order ~ 1.0 is obtained. These results give an idea of the way the total flux predictions would change if the constants of the model were not determined very accurately. It is comforting to see that the total flux hardly depends on the value of the perpendicular scale length, which is the parameter which probably would be most affected by larger uncertainties.

d) *The Ring Component*

Radio observations of the galactic plane (Burton 1976) as well as 2.4 μm flux result indicate that the galaxy has a high brightness, high density ring component with a radius of the order ~ $R_0 \sin \theta$ where $20 \leq \theta \leq 30$. Observations of the spiral galaxy M31 indicate that a bright ring of material of 50' radius is seen in H I, H II and radio continuum radiation; recent IRAS far IR (12, 25, 60 and 100 μm) observations also show this bright ring (Habing *et al.* 1984). It appears that high brightness, high density rings of this type are common features in spiral galaxies.

The ring which has been chosen to be the second component of the IR galaxy has been centred at a radius equal to $R_0 \sin 25$. The contribution of this

g at a point (R, Z) in the galaxy may be calculated m the density function:

$$\rho_{ring}(R,Z) = A\rho_0 \exp[-(R-R_{ring})^2/2s^2_{ring}]$$

$$\exp(-Z/Z_0) ,$$

ere this equation is valid for a specific spectral e and the following expression gives the ring lius $R_{ring} = R_0 \sin 25$. The parameters ρ_0 and refer to the local density and distance from the actic centre. The parameter Z_0, as for the disk e, represents the perpendicular scale heights different spectral types (see Table 1), the value s_{ring} has been fitted so as to reproduce the ervations (see section III), a value of 350 pc been obtained. The constant A is only a scale tor. The density at the centre of the ring is ıal to $\rho_{ring}(R_0 \sin 25) = A\rho_0$. Fits to the 2.4 μm x observations indicate that a value of A~ 7.3 is ɔropriate.

The effect of the ring component is only noticea- in the vicinity of the tangential points ($20 \leq l \leq 330 \leq l \leq 345$). This suggests the ring not to be ifferent entity from the disk, but only an enhan- nent of it.

Variations of the constants A, s_{ring} and R_{ring} uld clearly affect the amount of radiation contri- ted by the ring and its positional location. These anges will be more sensitive to variations of the rameter A than to variations of s_{ring}.

e) *The Spheroidal Component (Bulge)*

Analysis of the 2.2 μm observations close to the lactic centre (Bailey 1980; Allen, Hyland and nes 1983) reveal that the three dimensional ra- ıtion density from the bulge may be proportional $r^{-1.7} - r^{-1.8}$. Matsumoto *et al.* (1982) report 2.4 ı flux observations of the central region of the gal- y. They find that a representation of the bulge as a llection of oblate spheroids fits their observations propriately.

In this paper we shall adopt for the bulge the ıtsumoto *et al.* (1982) description. The bulge nsity at any point in the galaxy may be found as lows:

$$\rho_{bulge}(a) = B\rho_0 a^{-1.8} \text{ for } a \leq 0.2 \text{ kpc} ,$$

$$\rho_{bulge}(a) = B\rho_0 a^{-3.0} \text{ for } a \leq 0.2 \text{ kpc} ,$$

ıere

$$a^2 = R^2 + Z^2/(1 - e^2)$$

, R and Z represent the local density, the distance ɔm the galactic centre along the disk, and the rpendicular distance from the galactic plane. The rameter e represents the eccentricity of the family spheroids, and its value is equal to 0.6614 as determined by Matsumoto *et al.* (1982). This value of the eccentricity implies a minor to major axis ratio value of b/a ~ 0.75. The parameter B is a scale factor and is closely related to the bulge central density which is equal to $\rho_{centre} = B\rho_0$. Fits to the observational data indicate that B = 2.4 produces a good agreement. The Luminosity Function used for the Bulge component is the same one used for the disk (see Table A1), at present we are investigating the effects of other LF's for this galactic component.

III. MODEL FIT TO THE 2.4 μm OBSERVATIONS OF THE GALACTIC PLANE

Hayakawa *et al.* (1981) have conducted a full study of the 2.4 μm radiation along the galactic plane. They have published a longitude profile for the range $-70 \leq l \leq 60$ which we reproduce on Figure 1. As noted by Hayakawa *et al.* this profile shows a series of humps and depressions of which the most conspicuous are the humps located at $l \sim 25$ and $l \sim 340$. It also presents a strong central peak which correspond to the emission from the galactic bulge.

The mathematical model which we have described in section II was used in order to predict the emission of the galactic plane at 2.4 μm. Figure 1 shows the 2.4 μm flux data (filled circles), and the solid line represents the best model prediction. The contribution from different components were also calculated individually and their relative effects are shown in Figure 2; the solid line represents the disk contribution alone, the dashed line illustrates the ring prediction and finally the dot-dashed line shows the contribution of the bulge alone. The total sum of these three independent components results in the solid line illustrated in Figure 1. The predictions and the observational points show a remarkable agreement.

We mentioned before that the ring was to be taken only as an enhancement of the galactic disk so this is the reason why in the longitude intervals from $l \sim 20$ to 30 and from $l \sim 330$ to 345, the disk does not continue increasing monotonically. We assumed that the disk contribution remains constant in these longitude intervals and then it experiences a linear increment until it joins the original disk trend. The model predictions were calculated for different sets of model constants (A, B, h, and s_{ring}) and were superimposed on the observational data. The best prediction was chosen by eye. The values for the constants that characterise this "best prediction" are as follows:

i) Disk:

- ρ_0 depends on spectral type (see Table A1),
- $R_0 = 8.75$ kpc,

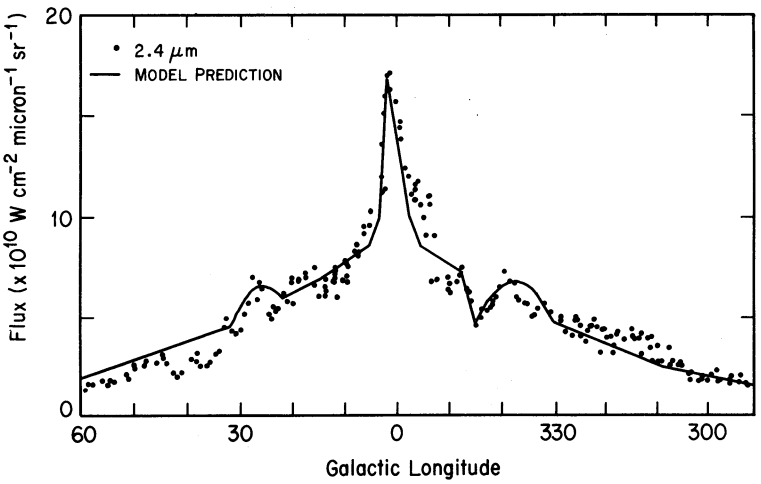

Fig. 1. Model prediction fit (solid line) to the 2.4 μm observations along the galactic plane. Filled circles are observations

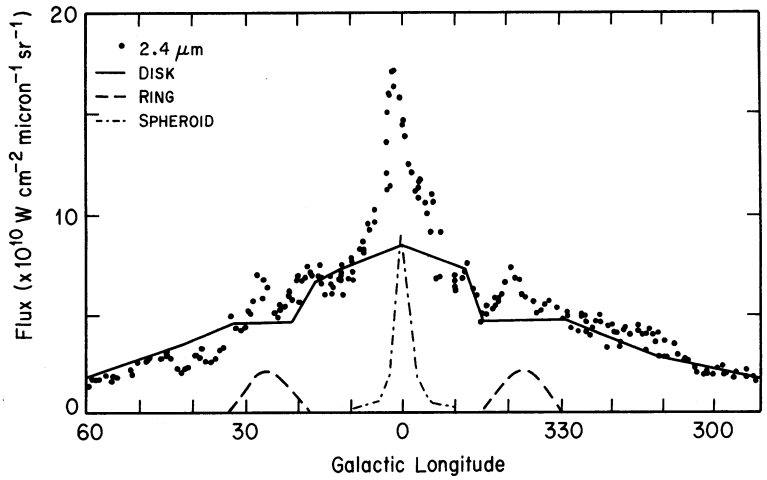

Fig. 2. The predicted 2.4 μm profiles is decomposed into its three components. Solid line is predicted disk; dashed line predicted ring; dot-dashed line, predicted spheroid. The addition of these components results in the solid line shown i Fig. 1.

– h = 2.5 kpc,
– Z_0 depends on spectral type (see Table A1).

ii) Absorption:
– $a_0(2.4\ \mu m) = 0.06$ mag kpc^{-1},
– $h_{abs} = 4$ kpc,
– $Z_{abs} = 0.1$ kpc.

iii) Ring:
– ρ_0 depends on spectral type (see Table A1),
– A = 7.3,
– $R_{ring} = 8.75 \sin 25 = 3.70$ kpc,
– $s_{ring} = 0.35$ kpc,
– Z_0 depends on spectral type (see Table A1).

iv) Spheroid:
– ρ_0 depends on spectral type (see Table A1),
– B = 2.4,
– e = 0.6614.

Our spheroid model predicts that at a distanc R~ 8 kpc, the ratio of the density of the bulge t that of the disk is equal to:

$$\rho_{bulge}(8)/\rho_{disk}(8) \sim 1/213 \ .$$

It is interesting to compare this ratio with tha quoted for optical data by Bahcall and Soneir (1980); their value is equal to:

$$\rho_{bulge}(8)/\rho_{disk}(8) \sim 1/800 \ .$$

This suggest that at the solar neighbourhood the relative importance of the disk to that of the bulge is approximately 4 times larger at visual magnitudes than it is at IR wavelengths. For the value $R_0 \sim 8.75$ kpc which we have adopted in this paper, this ratio becomes approximately:

$$\rho_{bulge}(8.75)/\rho_{disk}(8.75) \sim 1/279 \ .$$

IV. MISCELLANEOUS MAGNITUDE AND COLOUR PREDICTIONS OF THE IR MODEL OF THE GALAXY

In previous sections of this paper we have discussed the characteristics of the IR model of our galaxy. It was also established that a three component entity is an appropriate description of our system. Fits to the observed 2.4 μm galactic profiles allowed us to obtain a set of constants for the three components disk, ring and spheroid as well as for the distribution of the absorbing matter in the galaxy. In spite of the fact that the model and its predictions are completely determined by the mathematical expressions given in section III; we feel that a series of graphical examples of the model predictions at different positions in the galaxy would illustrate better the characteristics of the modelled IR stellar distribution in our galaxy. We shall produce predictions similar to those presented in Bahcall and Soneira (1980) for the visual components of our system so a direct

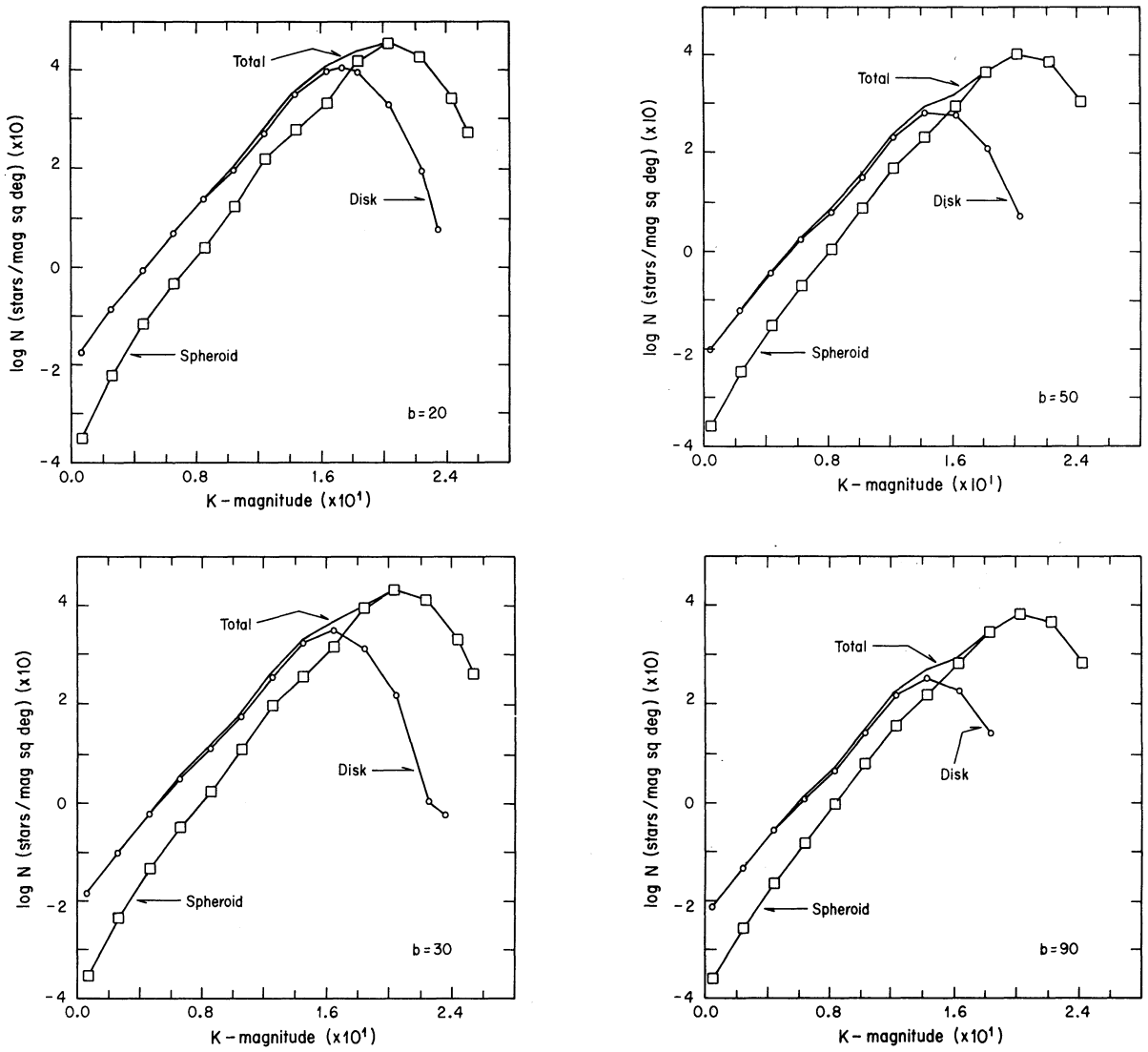

Fig. 3. Differential Counts Function averaged over galactic longitude at fixed galactic latitude: (a) b = 20, (b) b = 30, (3) b = 50, and (3) b = 90. Squares are spheroid; circles, disk.

comparison between the visual and the IR galaxy becomes possible.

a) *Latitude Dependence*

In Figure 3 we show diagrams of the mean Differential Counts Function (DCF) (Log of the number of stars per square degree in the magnitude interval m–1/2 to m + 1/2) at b = 20, 30, 50 and 90. The open dots represent the disk+ring contribution, the squares represent the spheroidal contribution alone, and the solid line illustrates the total (Spheroidal + Disk + Ring) contribution. These curves were obtained by using the standard IR model of the galaxy (See section II) with the constants derived in section III. Values of the stellar density every ten degrees in longitude were obtained at fixed latitude and finally were averaged to get the curves given in Figures 3a to 3d.

At bright K-magnitudes, the disk component dominated the DCF at all latitudes. At fainter magnitudes, the spheroidal component becomes dominant, it is interesting to notice that at b = 20, the spheroidal and disk contributions are equally important at $K \sim +18.0$, while at b = 90, this happens at $K \sim +15.0$. We may conclude that as we move away from the galactic plane, the spheroidal contribution effects on the DCF become more apparent due to the sharp density decay of the disk component.

The spheroidal contribution attains a maximum value at $K \sim +20.5$ for all latitudes. From that point onwards, there is an obvious decrease of the DCF which indicates that by this magnitude level we are already galaxy bounded and that those stars contributing to the faint end of the DCF must be intrinsically faint and should be located near-by.

The disk + ring contribution also shows a maximum which, however, shifts to brighter magnitudes as we progress towards higher galactic latitudes. Similar reasons as those mentioned for the spheroidal component indicate that by $K \sim +17.5$ for b = 20 and $K \sim +14.5$ for b = 90, the disk component is already galaxy bounded and that those stars which contribute to the faint end of the disk DCF must be located close-by and should be intrinsically faint.

The shift of the disk contribution towards brighter magnitudes, produces an interesting effect on the total DCF. A knee or a dip appears on the total DCF at or at a slightly fainter magnitude ($K \geq 16$) than that at which the disk attains its maximum. Should this knee appear on any observed DCF at galactic latitudes, it will constitute a useful point at which to separate the disk+ring contribution from that produced by the spheroidal component. Although it would be difficult to reach observationally due to the very faint K-magnitudes involved.

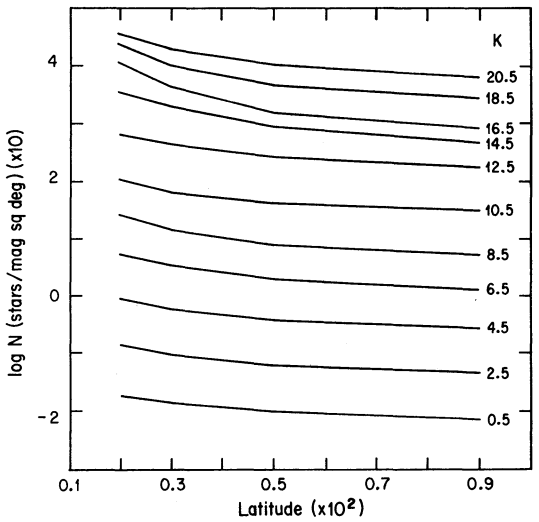

Fig. 4. Dependence of the Differential Counts Function with respect to galactic latitude averaged over galactic longitude for different K apparent magnitudes.

When we compare these figures with those given by Bahcall and Soneira (1980) for similar circumstances, the main difference is the fact that our curves reach a maximum and then decrease thereafter. For the V and B models the curves do not quite reach a maximum and certainly do not show any tendency to decrease.

On Figure 4 we show the decrease of the number of stars, at fixed magnitude, with respect to galactic latitude and averaged over galactic longitude. For all magnitudes there is a decay from low latitudes towards higher latitudes as was expected. However, the gradient for brighter magnitudes is much shallower than that at fainter magnitudes, this effect is also observed at visual and blue wavelengths (see Bahcall and Soneira 1980). This gradient has a value of ~ 0.9 in the logarithm at $K \sim 5.0$ compared with ~ 1.1 at $K \sim 10.5$ and ~ 1.6 at $K \sim 20.5$. The greater profusion of fainter magnitude stars at lower galactic latitudes is due to the spheroidal component.

It is interesting to notice that the increment per magnitude of the number of sources from $K \sim 0.5$ to $K \sim 10.5$ is more or less the same. From $K \sim 10.5$ to $K \sim 12.5$ there is a noticeable increase in this increment which may be explained by a steepening of the disk DCF in this magnitude range as is apparent from Figures 3a to 3d. This steepening may be produced by the sudden contribution, at this level, of more distant but intrinsically faint dwarf stars.

From $K \sim 12.5$ to $K \sim 20.5$ the increment per magnitude is smaller than at brighter magnitudes, and it shows a drastic minimum from $K \sim 14.5$ to

$K \sim 16.5$; this is due to the sudden lack of disk contribution which occurs at this level (see Figures 3a to 3d).

The slope of these curves is approximately equal for all magnitudes, at all latitudes, except at $K \geq 16.5$ and $b \leq 50$ where the slope is steeper due to the large contribution provided by the spheroidal component.

b) *Longitude Dependence*

On Figures 5a to 5d the dependence of the DCF at fixed latitudes (b = 20, 30, 50 and 70) with respect to galactic longitude is shown. At low b, the gradient between $l = 0$ and $l = 180$ increases monotonically from bright to faint magnitudes. At the fainter magnitudes ($K \sim 18.5$–20.5) the gradient is much steeper due to the faint source contribution of the spheroidal component. At b = 20 there is an interesting example of the relative importance of the disk and spheroidal components at faint magnitudes. Notice that the curves for $K \sim 16.5$ lies above that for $K \sim 18.5$ for $l \geq 100$ which indicates the sudden drop of faint disk sources. Again, the mean increment per magnitude from $K \sim 0.5$ to $K \sim 14.5$ is more or less constant at a given longitude. From $K \sim 14.5$ to $K \sim 20.5$ the increment per magnitude is much smaller, being this an effect of the lack of disk contribution at these magnitude levels.

When these curves are compared to the curves for the V and B cases (see Bahcall and Soneira 1980) the values of their slopes at faint and bright magnitudes are similar for the V, B and IR cases.

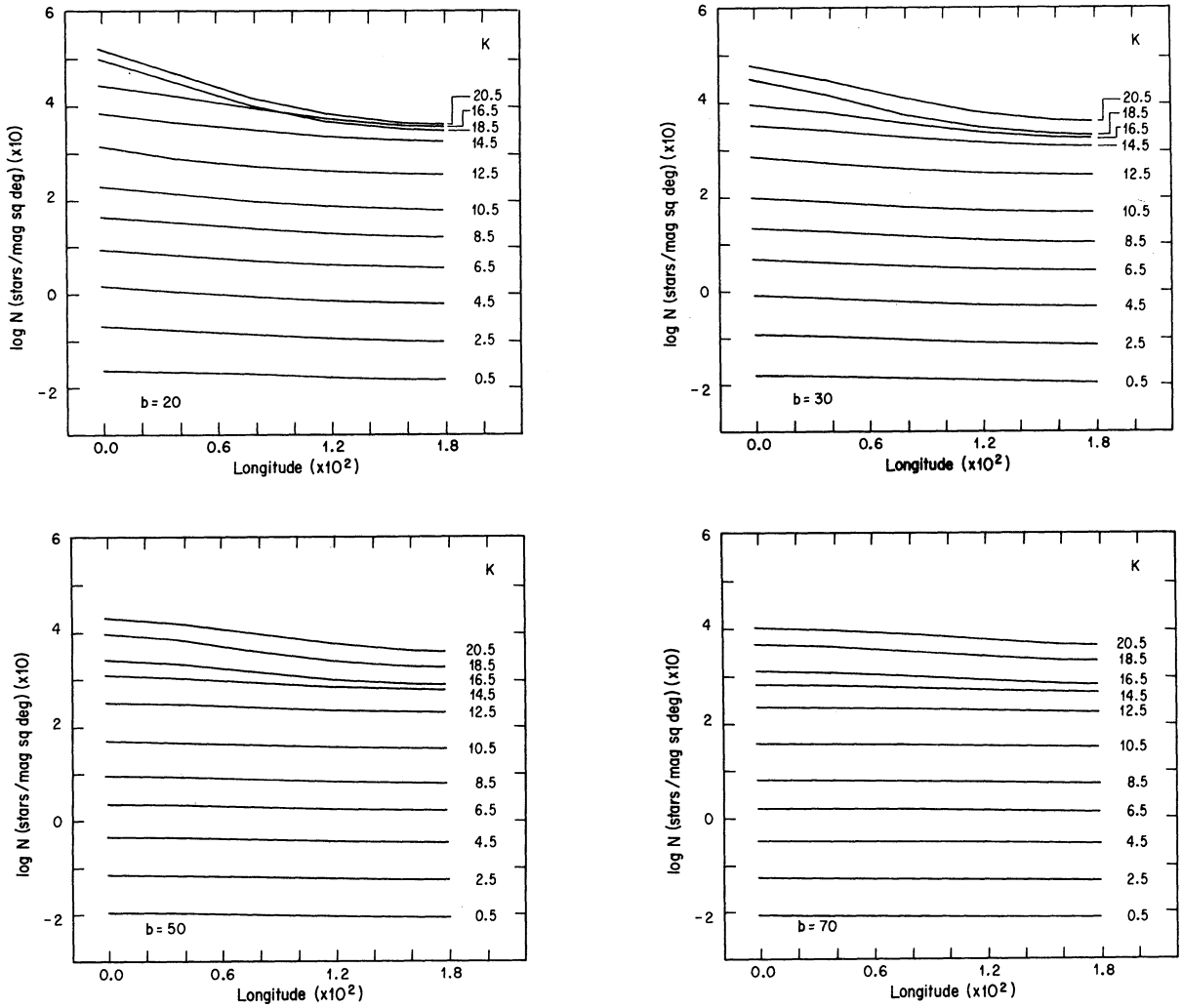

Fig. 5. Variation of the Differential Counts Function with respect to galactic longitude, at a fixed galactic latitude: (a) b = 20, (b) b = 30, (c) b = 50, and (d) b = 90.

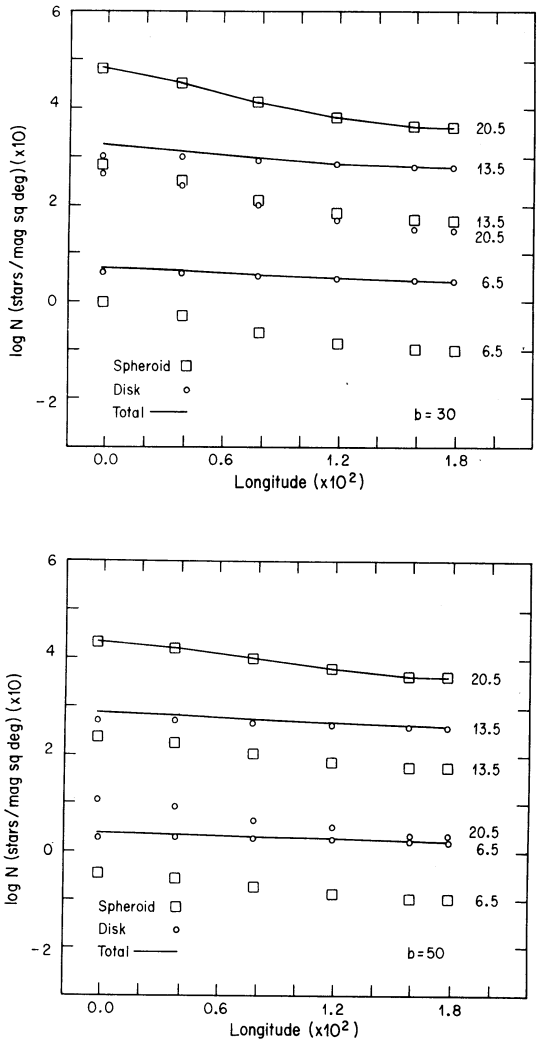

Fig. 6. Variation of the Differential Counts Function with respect to galactic longitude, at a fixed galactic latitude: (a) b = 30 and (b) b = 50. The total (solid line), spheroidal (squares) and disk (circles) contributions are shown for three different K-magnitudes.

Figures 6a and 6b show the DCF at three different magnitude levels; $K \sim 6.5$, $K \sim 13.5$ and $K \sim 20.5$ at b = 30 and b = 50 respectively. The spheroid contribution is represented by the squares, the open dots represent the disk + ring contribution and the solid line illustrates the total DCF. For both cases (b = 30, 50) the total DCF at brighter magnitudes ($K \sim 6.5$) is dominated by the disk component, whereas at fainter magnitudes ($K \sim 20.5$), the DCF is completely dominated by the spheroidal component. For the intermediate magnitude ($K \sim 13.5$) case, the total DCF at b + 30 and $l \geq 100$ is dominated by the disk component; for $l \leq 100$ even though the disk contribution remains quite important, the spheroidal component

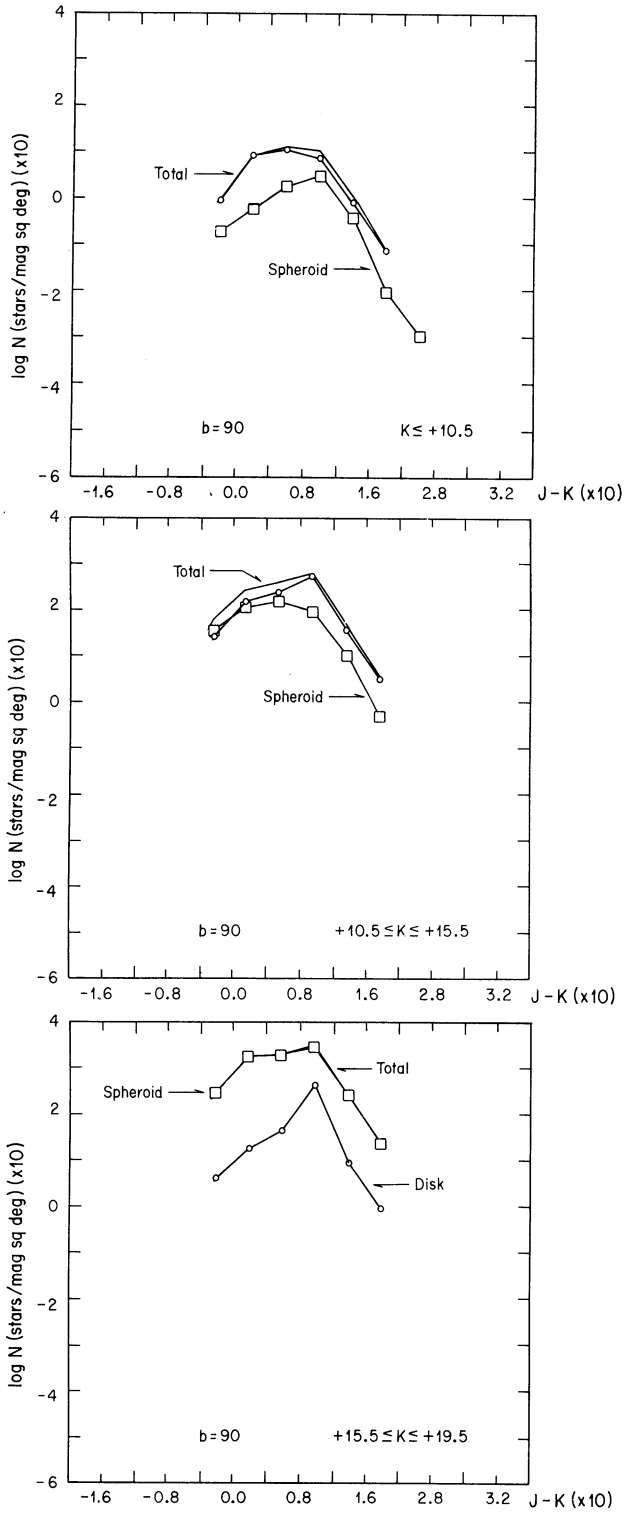

Fig. 7. Variation of the Differential Counts Function with respect to the J–K colour for stars in a fixed interval of K-magnitude. (a) $K \leq +10.5$, (b) $+10.5 \leq K \leq +15.5$ and (c) $+15.5 \leq K \leq +19.5$ in the direction of the galactic pole. The total, spheroidal (squares) and disk (circles) contributions are shown.

provides of the order of 10–20% to the total DCF. At b = 50; the spheroidal component provides 10–20% to the total DCF along the whole longitude range.

On Figures 7a to 7c graphs of the number of sources per square degree towards the galactic pole in the magnitude range $K \leq +10.5$, $+10.5 \leq K \leq +15.5$ and $+15.5 < K < +19.5$ are respectively shown. The spheroidal contribution is represented by the squares, the disk + ring contribution is illustrated by the open dots and the solid line represents the total contribution.

For the brighter sources $K \leq +10.5$, the disk component dominates the distribution in the range $-0.22 \leq J-K \leq +2.2$. The disk component reveals a maximum at $J-K \sim 0.6$ while the spheroidal component has a maximum at $J-K \sim 1.0$.

For the sources in the magnitude interval $+10.5 \leq K \leq +15.5$, the disk and the spheroidal components contribute approximately equal amounts in the range $J-K \leq 0.2$. For redder colours ($J-K \geq 0.2$), the dominant component is the disk. This fact may be explained by the large number of late spectral type dwarf stars which begin to produce sizeable contributions at this brightness level. The maximum of the spheroidal component appears at $J-K \sim 0.6$, which is ~ 0.4 mag bluer than the maximum for the brighter stars (see Fig 7a). A sharp maximum at $J-K \sim 1.0$ is predicted for the disk component; which is ~ 0.4 redder than the maximum for the brighter stars (see Fig. 7a). The relative sharpness of this maximum provides unquestionable evidence of the increasing importance of the late type dwarf stars towards fainter magnitudes.

For the magnitude range $+15.5 \leq K \leq +19.5$, the whole colour interval ($-0.22 \leq J-K < +1.8$) is dominated by the spheroidal component. A mildly sharp maximum and a very sharp maximum for the spheroidal and disk components respectively are obtained at $J-K \sim 1.0$; these maxima are due to the late type dwarf stars which become increasingly important towards fainter magnitudes.

It is interesting to comment on the relative colour position of the maxima for the different components (disk and spheroid) on Figures 7a to 7c . Since no difference in the LF is used for the disk and spheroid, it is solely an effect produced by the different geometrical arrangements of these components as seen from the Sun.

V. MODEL FITS TO SELECTED CCFs FROM THE LITERATURE

In this section we shall use the global IR model derived from our fit to the 2.4 μm observations to predict the CCF in different directions along the galactic plane for which there are 2.2 μm counts available in the literature.

Table 1 gives in column 1 a number identifying the region to be studied, columns 2 and 3 give respectively the galactic longitude and latitude of the regions, and column 4 identifies the literature sources of the observational counts.

TABLE 1

REGIONS TO BE STUDIED

Region	Longitude	Latitude	Source[a]
38	15.0	0.0	3
35	26.5	0.0	5
39	27.0	0.0	3
31	40.0	0.0	2,4
40	40.0	0.0	3
32	50.0	0.0	2,4
33	60.0	0.0	2,4
34	305.0	0.0	6
37	350.0	0.0	3
36	359.5	0.0	3

a. Sources: 1) Ruelas-Mayorga 1990b. 2) Neugebauer and Leighton 1969. 3) Kawara *et al.* 1982. 4) Eaton, Adams and Giles 1984. 5) Mikami *et al.* 1982. 6) Danks *et al.* 1984.

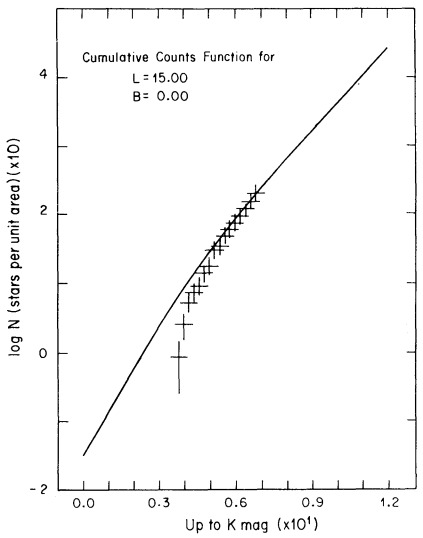

Fig. 8. Observed Cumulative Counts Functions (CCFs) for selected areas. The crosses indicate the observational points which have been collected from the literature. The galactic coordinates of each region are: longitude = DD. MM, latitude = ±DD.MM. The solid line represents the IR galactic model prediction with: R_0 = 8.75 kpc, radius within which the disk does not contribute to the counts = 0.0 kpc, stellar radial scale length = 2.50 kpc, local absorption parameter for the K-magnitude = 0.08 mag kpc^{-1}, angular aperture of the simulated telescope = 1.13°, number of square degrees used in the simulation = 1.0 sqdeg.

In Figures 8 to 17, the crosses stand for the observational points. Vertical error bars that

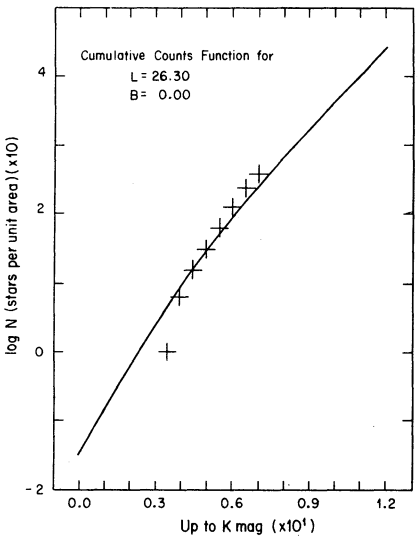

Fig. 9. Same as Fig. 8.

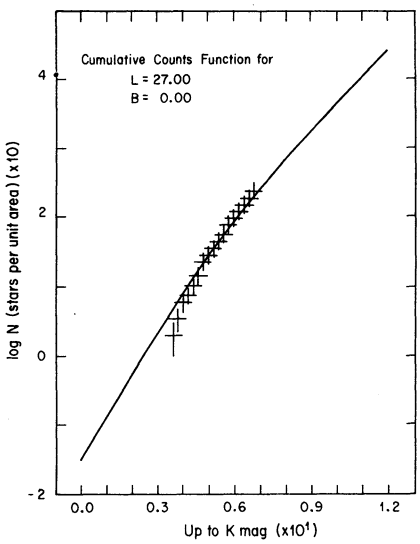

Fig. 10. Same as Fig. 8.

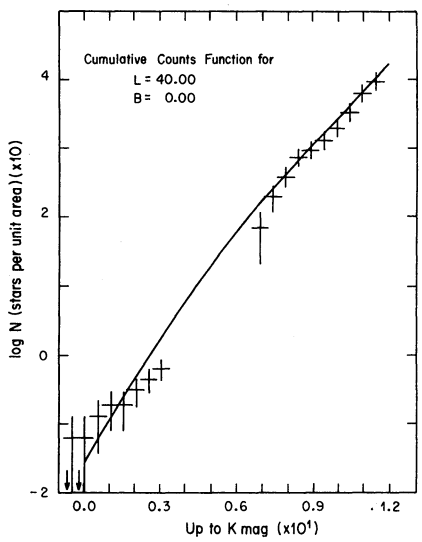

Fig. 11. Same as Fig. 8.

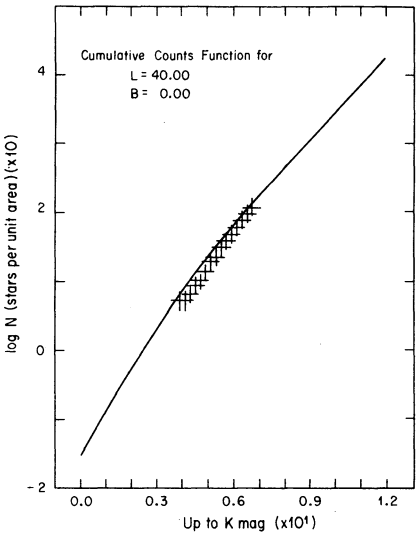

Fig. 12. Same as Fig. 8.

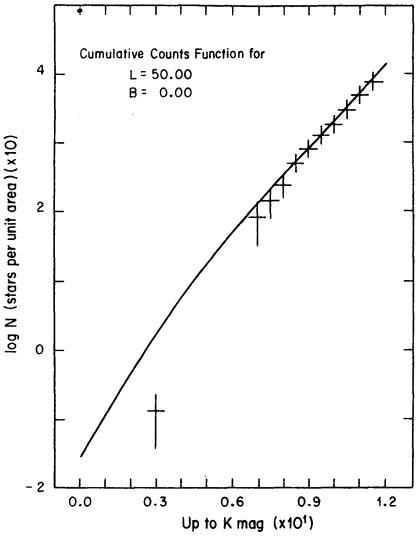

Fig. 13. Same as Fig. 8.

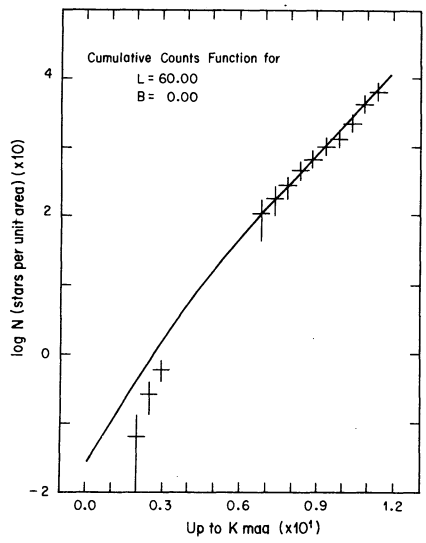

Fig. 14. Same as Fig. 8.

correspond to the statistical uncertainties ($n^{1/2}$) for each observational point have been plotted. At faint levels the error bars are typically smaller than the size of the symbol. The horizontal error bars represent a magnitude uncertainty which has been estimated to be of the order ± 0.3 magnitudes. The solid line represents the theoretical CCF predicted by the model in the direction under study.

Figure 8 illustrates the data and theoretical fit to a region on the galactic plane at $l \sim 15$. We notice that the model agrees well with the observations at faint magnitudes. At brighter magnitudes there is a tendency for the model to be above the observational points. Golisch (1983) on the basis of two regions only, notes that the Jones *et al.* (1981) model also tends to predict more sources at brighter magnitudes than there are observed. Golisch proposes a revised disk model in which the early M giants stars have brighter absolute K magnitudes, and the later M giants have fainter absolute K magnitudes. With this revised model he is successful in fitting the observations at $l = 10$, b = +1 at the bright and faint magnitude levels, however his revised model is not appropriate for the intermediate magnitude range, for which the predictions turn out to be deficient with respect to the observations. The nature of the data in this region is mainly of intermediate magnitude nature, and the remarkable agreement between the model and the observations in the

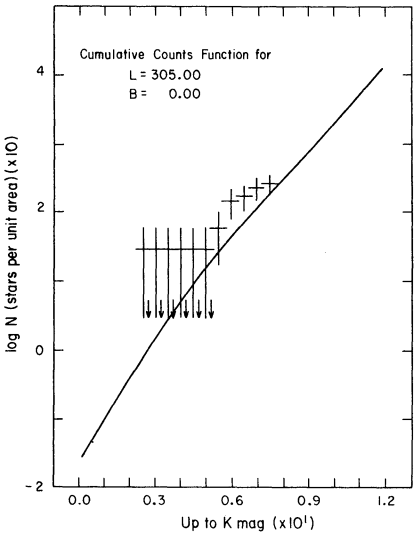

Fig. 15. Same as Fig. 8.

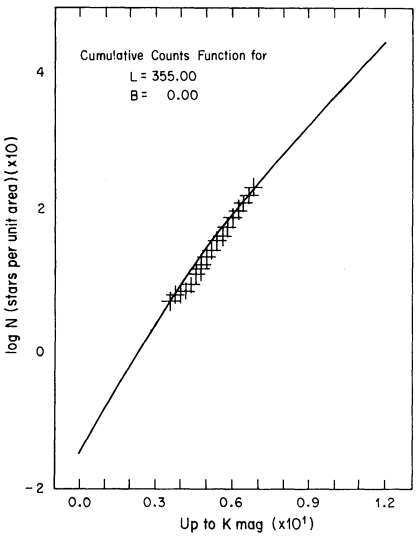

Fig. 16. Same as Fig. 8.

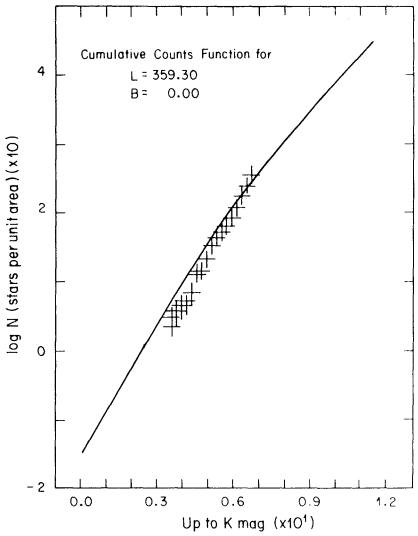

Fig. 17. Same as Fig. 8.

range $5.0 \leq K \leq 7.0$, suggests that the bright magnitude discrepancy may be due to a different effect which we do not understand as yet. At present we are engaged in exploring several different model alterations, including changes in absolute magnitude, radial scale length for different spectral types and Luminosity Functions, which could eventually prove to produce better fits to the observations.

The observations shown in Figures 9 and 10 (l = 26.5 and l = 27) agree well with the model, except for a small discrepancy, where the model predicts slightly more sources at the bright end than are observed.

Figures 11, to 14 illustrate the model predictions and the observations for the regions at l = 40, 50 and 60. The agreement between the model and the observations at the faint end is very good. At the bright magnitudes of l = 50, 60, however, there is a noticeable excess of the model prediction over the observational data.

The observational points presented in Figure 15 for l = 305, have been taken from Danks *et al.* (1984). It is clear that the model predictions are deficient with respect to the observations. The work of Danks *et al.* indicates that two new clusters of stars have been discovered in this area; therefore it is probable that this local concentration of objects is responsible for the difference between the observed and predicted CCFs (see the figures in Danks et al., 1984).

Finally, data for l = 355, b = 0 and l = 359.5, b = 0, taken from Kawara *et al.* (1982), are illustrated in Figures 16 and 17. The agreement of the model predictions with the observations is remarkable for both regions. Note that the observed CCF in Figure 17 appears to have a slightly steeper slope than the prediction of the model.

VI. CONCLUSIONS

The IR model of the galaxy described in detail in section II was used to predict stellar counts which were then compared with observations of stellar counts taken from the literature at different positions along the galactic plane. Based on the result presented in this paper, and those which will be presented in two forthcoming papers (Ruelas-Mayorga 1991b; Ruelas-Mayorga and Teague 1991), it is possible to say that the model has proved to provide an adequate description of the distribution in the galaxy of the IR stellar population.

Our IR model of the galaxy should prove useful, when compared with observations, in identifying slight variations and clumpiness of the absorbing material in certain directions in the galaxy, identifying the IR counterparts to objects with poorly known positions, such as OH/IR objects, for which a precise knowledge of background radiation due to galactic stars is necessary, the model could also be used in predicting the radiation and counts background against dark clouds so that embedded objects could be identified more readily. It could also be used in searches for other background sources such as the interplanetary dust and the zodiacal light. Finally, the appearance of our galaxy derived from our model enables a comparison with observations of external galaxies whose overall structure is better known.

The author would like to acknowledge the financial help provided by Consejo Nacional de Ciencia y Tecnología and that provided by the

Australian National University during the course of this research. Many useful discussions with A. R. Hyland, T.J. Jones, R. Wainscoat, M. Casali and J. Elso are also acknowledged. I also acknowlegde the help and suggestions provided by S. Torres-Peimbert and the excellent typing skills of E. Themsel. Finally the author would like to thank the department of Astronomy at New Mexico State University and the Instituto de Astronomía, UNAM for their kindness and help during difficult moments.

REFERENCES

Allen, C.W.1973, Astrophysical Quantities, 3rd (London: Athlone Press).
Allen, D.A.Hyland, A.R., and Jones, T.J. 1983, *M.N.R.A.S.*, **204**, 1145.
Bahcall, J.N. and Soneira, R.M. 1980, *Ap. J. Suppl.*, **44**, 73.
Bailey, M.E. 1980, *M.N.R.A.S.*, **190**, 217.
Becklin, E.E. and Neugebauer, G. 1968, *Ap. J.*, **151**, 145.
Blaauw, A. 1963, in *Stars and Stellar Systems (Basic Astronomical Data)*, vol. **III**, 383.
Boissé, P. *et al.* 1981, *Astr. and Ap.*, **94**, 265.
Burton, J.B. 1976, *Ann. Rev. Astr. and Ap.*, **14**, 275.
Danks, A.C., Wamsteker, W., Shaver, P.A., and Retallack, D.S. 1984, *Astr. and Ap.*, **132**, 301.
de Vaucouleurs, G. 1959, in *Handbuch der Physik*, vol. **53**, ed. S. Flügge (Berlin: Springer-Verlag), p. 311.
Eaton, J.H., Adams, D.J., and Giles, A.B.,1984, *M.N.R.A.S.*, **208**, 241.
Elias, J.H. 1978a, *A.J.*, **83**, 791.
Elias, J.H. 1978b, *Ap. J.*, **223**, 859.
Faber, S.M., Burstein, D., Tinsley, B.M., and King, I.R. 1976, *Ap. J.*, **81**, 45.
Freeman, K.C. 1970, *Ap. J.*, **160**, 811.
Gilmore, G. and Reid, N. 1983, *M.N.R.A.S.*, **202**, 1025.
Golisch, W.F. 1983, Master's Thesis. University of Minnesota.
Graham, J.A. 1979, *IAU Symposium No. 84, The Large Scale Characteristics of the Galaxy*, ed. W.B. Burton (Dordrecht: D. Reidel), p. 195.
Habing, H.J. 1984, *Ap. J. (Letters)*, **278**, L59
Hayakawa, S., Ito, K., Matsumoto, T., Ono, T., and Uyama, K. 1976, *Nature*, **261**, 29.
Hayakawa, S., Ito, K., Matsumoto, T., and Uyama, K. 1977, *Astr. and Ap.*, **58**, 325.
Hayakawa, S. *et al.* 1979a, *Nature*, **271**, 510.
Hayakawa, S. *et al.* 1979b, *New Zealand Journal of Science*, **22**, 353.
Hayakawa, S. *et al.* 1981, *Astr. and Ap.*, **100**, 116.
Hiromoto, N., Maihara, T., Oda, N., and Okuda, H. 1983, *Pub. Astr. Soc. Japan*, **35**, 413.
Hofman W., Lemke, D., and Thum, C. 1977, *Astr. and Ap.*, **57**, 111.
Humphreys, R.M. 1978, *Ap. J. Suppl.*, **38**, 309.
Ishida, K. and Mikami, T. 1982, *Pub. Astr. Soc. Japan*, **34**, 89.
Ito, K., Matsumoto, T., and Uyama, K. 1976, *Pub. Astr. Soc. Japan*, **28**, 427.
Ito, K., Matsumoto, T., and Uyama, K. 1977, *Nature*, **265**, 517.
Johnson, H.L. 1968, *Stars and Stellar Systems (Nebulae and Interstellar Matter)*, vol. **VII**, 167.
Jones, T.J. and Hyland, A.R. 1980, *M.N.R.A.S.*, **192**, 359.
Jones, T.J., Ashley, M., Hyland, A.R., and Ruelas-Mayorga, A. 1981, *M.N.R.A.S.*, **197**, 413.
Kawara, K. *et al.* 1982, *Pub. Astr. Soc. Japan*, **34**, 389.
Kormendy, J. 1977a, *Ap. J.*, **214**, 359.
Kormendy, J. 1977b, *Ap. J.*, **218**, 333.
Lockman, F.J. 1977, *A.J.*, **82**, 408.
Lockman, F.J. 1979, *Ap. J.*, **232**, 761.
Lyngå, G. and Ruelas-Mayorga, R.A. 1979, (Private Communication).
Maihara, T., Oda, N., and Okuda, H. 1979, *Ap. J. (Letters)*, **227**, L129.
Maihara, T., Oda, N., Shibai, H., and Okuda, H. 1981, *Astr. and Ap.*, **97**, 139.
Maihara, T., Oda, N., Sugiyama, T., and Okuda, H., 1981, *Astr. and Ap.*, **97**, 139.
Matsumoto, H. *et al.* 1982, in *The Galactic Center, AIP Conference Proceedings No. 83*, eds. G. R. Riegler and R. D. Blandford, p. 48.
Mikami, T. and Ishida, K. 1981, *Pub. Astr. Soc. Japan*, **33**, 135.
Mikami, T., Ishida, K., Hamajima, K., and Kawara, K. 1982, *Pub. Astr. Soc. Japan*, **34**, 223.
Neugebauer, G. and Leighton, R.B. 1969, *Two-Micron Sky Survey. A Preliminary Catalog*, NASA SP-3047.
Nishimura, T., Low, F.J., and Kurtz, R.F. 1980, *Ap. J. (Letters)*, **239**, L101.
Okuda, H. 1980, *IAU Symposium No. 96, Infrared Astronomy*, eds. C.G. Wynn Williams and D.P. Cruikshank (Dordrecht: D. Reidel) p. 247.
Ruelas-Mayorga, R.A. 1991b, *Rev. Mexicana Astron. Astrof.*, **22**, 43.
Ruelas-Mayorga, R.A. and Teague, P.F. 1991c, *Astr. and Ap.*, submitted.
van der Kruit, P. C. and Freeman, K.C. 1984, *Ap. J.*, **278**, 81.
van der Kruit, P.C. and Searle L. 1981a, *Astr. and Ap.*, **95**, 105.
van der Kruit, P.C. and Searle L. 1981b, *Astr. and Ap.*, **95**, 116.
van der Kruit, P.C. and Searle L. 1982a, *Astr. and Ap.*, **110**, 61.
van der Kruit, P.C. and Searle L. 1982b, *Astr. and Ap.*, **110**, 79.

APPENDIX

LUMINOSITY FUNCTIONS AND ABSORPTION COEFFICIENTS FOR DIFFERENT WAVELENGTHS

In this Appendix we have gathered in Table A1 the Luminosity Function data for the follow-

TABLE A1

LUMINOSITY FUNCTION MAGNITUDES AND COLOURS

Sp. Type	log (ρ_0)	Z_0	B	V	J	H	K	2.4μm	$B-V$	$V-K$	$J-H$	$H-K$	$J-K$	σ
B0,1 V	2.95	0.04	-4.27	-3.99	-3.34	-3.26	-3.12	-3.11	-0.28	-0.87	-0.08	-0.14	-0.22	0.50
B2,3 V	3.83	0.04	-2.23	-2.01	-1.51	-1.44	-1.33	-1.32	-0.22	-0.68	-0.07	-0.11	-0.18	0.50
B5 V	4.09	0.04	-1.16	-1.00	-0.65	-0.60	-0.53	-0.52	-0.16	-0.47	-0.05	-0.07	-0.12	0.50
B8-A0 V	5.33	0.07	0.15	0.20	0.29	0.31	0.34	0.34	-0.05	-0.14	-0.02	-0.03	-0.05	0.50
A2-5 V	5.54	0.10	1.68	1.58	1.39	1.32	1.33	1.33	0.10	0.25	0.07	-0.01	0.06	0.40
F0-5 V	6.09	0.14	3.37	2.94	2.15	1.90	1.87	1.87	0.43	1.07	0.25	0.03	0.28	0.50
F8-G2 V	6.39	0.25	5.01	4.49	3.46	3.19	3.14	3.14	0.52	1.35	0.27	0.05	0.32	0.30
G5 V	6.50	0.30	5.66	5.00	3.86	3.55	3.51	3.52	0.66	1.49	0.31	0.04	0.35	0.30
G8-K3 V	7.00	0.35	6.85	6.02	4.62	4.22	4.15	4.18	0.83	1.87	0.40	0.07	0.47	0.50
K4-5 V	7.05	0.30	8.40	7.25	5.21	4.61	4.50	4.54	1.15	2.75	0.60	0.11	0.71	0.50
M0-1 V	7.15	0.30	10.23	8.78	5.89	5.14	5.00	5.04	1.45	3.78	0.75	0.14	0.89	0.50
M2-3 V	7.25	0.30	11.46	9.92	6.41	5.69	5.50	5.51	1.54	4.42	0.72	0.19	0.91	0.50
M4-5 V	7.35	0.30	13.11	11.52	7.40	6.73	6.50	6.49	1.59	5.02	0.67	0.23	0.90	1.00
F8-G2 III	4.65	0.50	3.45	2.53	1.01	0.50	0.45	0.41	0.92	2.08	0.51	0.05	0.56	1.00
G5 III	4.65	0.50	2.92	2.00	0.48	-0.03	-0.08	-0.05	0.92	2.08	0.51	-0.05	0.46	1.00
G8 III	5.20	0.25	2.55	1.60	0.03	-0.50	-0.56	-0.52	0.95	2.16	0.53	-0.06	0.47	0.80
K0,1 III	5.59	0.20	2.69	1.62	-0.14	-0.72	-0.80	-0.72	1.07	2.42	0.58	0.08	0.66	0.70
K2,3 III	5.23	0.20	2.33	1.10	-0.90	-1.55	-1.66	-1.55	1.23	2.76	0.65	0.11	0.76	0.70
K4,5 III	4.28	0.30	1.58	0.10	-2.44	-3.22	-3.36	-3.22	1.48	3.46	0.78	0.14	0.92	0.60
M0 III	3.48	0.30	1.20	-0.35	-3.17	-3.98	-4.14	-3.97	1.55	3.79	0.81	0.16	0.97	0.60
M1 III	3.13	0.30	1.08	-0.48	-3.38	-4.23	-4.40	-4.22	1.56	3.92	0.85	0.17	1.02	0.60
M2 III	3.13	0.30	0.94	-0.65	-3.73	-4.58	-4.76	-4.57	1.59	4.11	0.85	0.18	1.03	0.60
M3 III	3.13	0.30	0.95	-0.65	-4.16	-5.03	-5.23	-5.02	1.60	4.58	0.87	0.20	1.07	0.60
M4 III	3.00	0.30	0.79	-0.80	-5.06	-5.81	-6.04	-5.82	1.59	5.24	0.75	0.23	0.98	0.60
M5 III	3.00	0.30	0.71	-0.84	-5.88	-6.64	-6.90	-5.86	1.55	6.06	0.76	0.26	1.02	0.50
M6 III	2.45	0.30	0.65	-0.89	-6.75	-7.60	-7.90	-7.66	1.54	7.01	0.85	0.30	1.15	0.50
M7 III	2.09	0.30	0.60	-1.00	-7.70	-8.57	-8.90	-8.65	1.60	7.90	0.87	0.33	1.20	0.50
M8 + III	1.65	0.30	0.50	-1.10	-8.60	-9.53	-9.90	-9.64	1.60	8.80	0.93	0.37	1.30	0.50
young OB	2.61	0.05	-5.30	-5.14	-4.80	-4.76	-4.70	-4.69	-0.16	-0.44	-0.04	-0.06	-0.10	1.20
A-G I-II	1.53	0.05	-5.62	-6.05	-6.72	-6.85	-7.00	-6.99	0.43	0.95	0.13	0.15	0.28	2.00
K-M2 I-II	1.49	0.05	-4.93	-6.37	-8.68	-9.30	-9.50	-9.30	1.44	3.13	0.62	0.20	0.82	1.00
M3-4 I-II	1.10	0.05	-4.45	-6.09	-9.98	-10.74	-11.00	-10.73	1.64	4.91	0.76	0.26	1.02	1.00

ing wavelengths: *B, V, J, H, K*, 2.4 μm, *B–V, V–K, J–H, H–K*, and *J–K*. Column 1 gives the spectral type and the luminosity class, column 2 shows the logarithm of the number density of that stellar type at the solar neighbourhood in stars kpc^{-3}, column 3 gives the value of the characteristic height in kpc for that spectral type above the galactic plane. Columns 4 to 14 shows the magnitude and colour values, and finally column 15 gives the dispersion in magnitudes around the central values given in columns 4 to 14. Table A2 gives the values of the local absorption parameters for each one of the wavelengths considered in this appendix.

TABLE A2

LOCAL ABSORPTION PARAMETERS

λ	a(λ) (mag kpc^{-1})	λ	a(λ) (mag kpc^{-1})
B	1.30	$B-V$	0.30
V	1.00	$V-K$	0.96
J	0.33	$J-H$	0.10
H	0.16	$H-K$	0.08
K	0.08	$J-K$	0.18
2.4 μm	0.06	....	....

R.A. Ruelas-Mayorga: Instituto de Astronomía, UNAM, Apartado Postal 70-264, 04510 México, D.F., México.